Journal of Colloid and Interface Science 664 (2024) 1031–1041

Contents lists available at ScienceDirect

Journal of Colloid And Interface Science

journal homepage: www.elsevier.com/locate/jcis

Regular Article

# Unlocking new dimensions in long-acting injectables using lipid mesophase-based beads

Elena Allegritti [a], Luisa Giansanti [a], Gregor Bordon [b], Maria Anna Maggi [c], Paola Luciani [b,*], Simone Aleandri [b,*]

[a] Dipartimento di Scienze Fisiche e Chimiche, Università degli Studi dell'Aquila, 67100 Coppito, L'Aquila, Italy
[b] Department of Chemistry, Biochemistry and Pharmaceutical Sciences, University of Bern, 3012 Bern, Switzerland
[c] Hortus Novus, Canistro, 67051 L'Aquila, Italy

## GRAPHICAL ABSTRACT

Unleashing the potential of lipid mesophase-based beads as a long-acting platform to deliver hydrophilic and lipophilic drugs: our study investigates their physico-chemical properties using four model drugs, revealing the ability to customize bead topology and their properties by adjusting the lipid mixture composition. This may be a promising landscape for an innovative drug delivery approach.

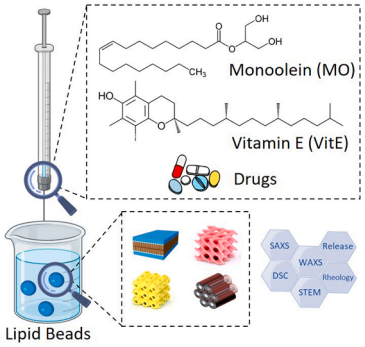


## ARTICLE INFO

*Keywords:*
Beads
Drug delivery
Mesophases
Sustained release profile

## ABSTRACT

In this study, we explored the use of lipid mesophases (LMPs) as a biocompatible and biodegradable material for sustained drug delivery. Our hypothesis centered on leveraging the high surface-to-volume ratio of LMP-based beads to enhance strength, stability, and surface interaction compared to the LMP bulk gel. To modulate drug release, we introduced antioxidant vitamin E into the beads, influencing mesophase topologies and controlling drug diffusion coefficients. Four drugs with distinct chemical properties and intended for three different pathologies and administration routes were successfully loaded into the beads with a drug entrapment efficiency exceeding 80 %. Notably, our findings revealed sustained drug release, irrespective of the drugs' chemical properties, culminating in the development of an injectable formulation. This formulation allows direct

*Abbreviations:* LMPs, lipid mesophases; MO, monoolein; L, lamellar phase; Q, bicontinuous cubic phase; $H_{II}$, inverse hexagonal phase; I, micellar phase; TOFA, tofacitinib citrate; RAPA, rapamycin; GEFI, gefitinib; BUPI, bupivacaine; VitE, vitamin E; SAXS, small-angle X-ray scattering; WAXS, wide-angle X-ray scattering; *a*, lattice parameter; DSC, differential scanning calorimetry; MO-B, MO-based beads; MO/VitE-B, $H_{II}$-based beads; STEM, scanning transmission electron microscope; LVR, linear viscoelastic region; *d*, diffusion coefficient; SF, simulated fluid..

* Corresponding authors.
*E-mail addresses:* paola.luciani@unibe.ch (P. Luciani), simone.aleandri@unibe.ch (S. Aleandri).

https://doi.org/10.1016/j.jcis.2024.03.067
Received 15 January 2024; Received in revised form 4 March 2024; Accepted 10 March 2024
Available online 12 March 2024

administration into the target site, minimizing systemic exposure, and thereby mitigating adverse effects. Our approach demonstrates the potential of LMP-based beads for tailored drug delivery systems with broad applications in diverse therapeutic scenarios.

## 1. Introduction

Non-lamellar lipid phases are acknowledged to play a plethora of different biological functions[1–3] and, thanks to their unique material properties and functionality, complementary to lamellar lipid systems, are gaining momentum as versatile drug carriers.[4–7] Lipid mesophases (LMPs) are thermodynamically stable structures and, thanks to their high degree of order, they are less prone to fusion, leakage or aggregation compared to other lipid-based drug delivery systems.[8] Compared to lamellar vesicles such as liposomes, for instance, the ordered arrangement of lipids in the mesophase allows for a more efficient packing of drugs, increasing either their loading capacity and/or their retention into the gel.[9] Conveniently, LMPs are prepared following a straightforward process, mixing monoacyl glycerol lipids such as monoolein (MO, recognized as safe for human and animal use by US Food and Drug Administration) and water.

Increasing the water content, the flat lipid bilayers of a lamellar phase (L) transform into a curved bicontinuous cubic phase (Q; with Ia3d, Pn3m or Im3m geometry), while the presence of additives, such as the antioxidant vitamin E (VitE) [10–15], promotes the formation of highly viscous inverted hexagonal ($H_{II}$) and micellar phases (I) at room temperature [16], which consist of hexagonally packed water channels surrounded by lipids [17] and inverse micellar phase consists of 3D packings of discrete inverse micellar aggregates, respectively.[1819].

In contrast to other gel-based drug carriers, LMPs could avoid the initial burst release due to the swelling process [20] as the less viscous and injectable L phase (formed at low water percentages) has also a lower diffusion coefficient with respect to more hydrated topologies [2116].

Traditionally, LMP-based drug delivery systems have been either bulk gels or polymer-stabilized nano dispersions known as cubosomes. [22,23] To gain strength, stability, and structural integrity thanks to a higher surface/volume ratio than LMP gels and to streamline the manufacturing process than cubosomes, we propose here LMPs-based beads to be injected locally. A plethora of different drugs can be encapsulated beneath the surface of microbeads and, differently from what observed in bulk LMP gels, drug release from beads is not only driven by diffusion, but also by controlling the beads' porosity and erosion.

Spanning from tofacitinib citrate (TOFA, a hydrophilic Janus kinase inhibitor),[24,25] to rapamycin (RAPA, a hydrophobic immunosuppressant),[26–29] via gefitinib (GEFI, a hydrophobic anti-tumor drug proposed for the treatment of metastatic colorectal cancer)[30–33] and bupivacaine (BUPI, a potent amphiphilic local anesthetic)[32,34–36], our injectable LMP beads are based on a blend of MO, water, and the antioxidant VitE, as depicted in Scheme 1.

This patient-centric drug delivery platform, manufactured to maximize the drug concentration at the site of injection and to minimize adverse reactions, was developed with the aid of an in-depth physicochemical characterization of the beads *via* small and wide-angle X-ray scattering (SAXS and WAXS, respectively).

The X-rays scattered by the gel give a set of maxima that correspond to sharp Bragg reflections, characteristic of the long-range positional order, peculiar for each geometry (a list of Bragg reflections identifying the symmetry of the mesophase are reported in Scheme 1). Moreover, rheology, differential scanning calorimetry (DSC), optical and electron microscopy were used to elucidate the macroscopical and thermal features of the ensuing beads. The high percentages of the loaded drugs (up to 80 %) did not induce any change in the symmetry with respect to the bulk gel.[15,37] The self-assembly features of the formulations were correlated to the drug release profiles of the four drugs and, independently of the nature (size and polarity) of the active principles, the sustained release could be ascribed to the internal 3D matrix of the beads. The injectability of the beads, possible despite their macroscopic dimensions, proves the versatility of this drug delivery platform for parenteral use. The achieved sustained release profiles, obtained both in physiological conditions and simulated fluids, persist even upon lipase-triggered dissolution of the beads, as MO can reorganize into vesicles, effectively encapsulating hydrophobic molecules.

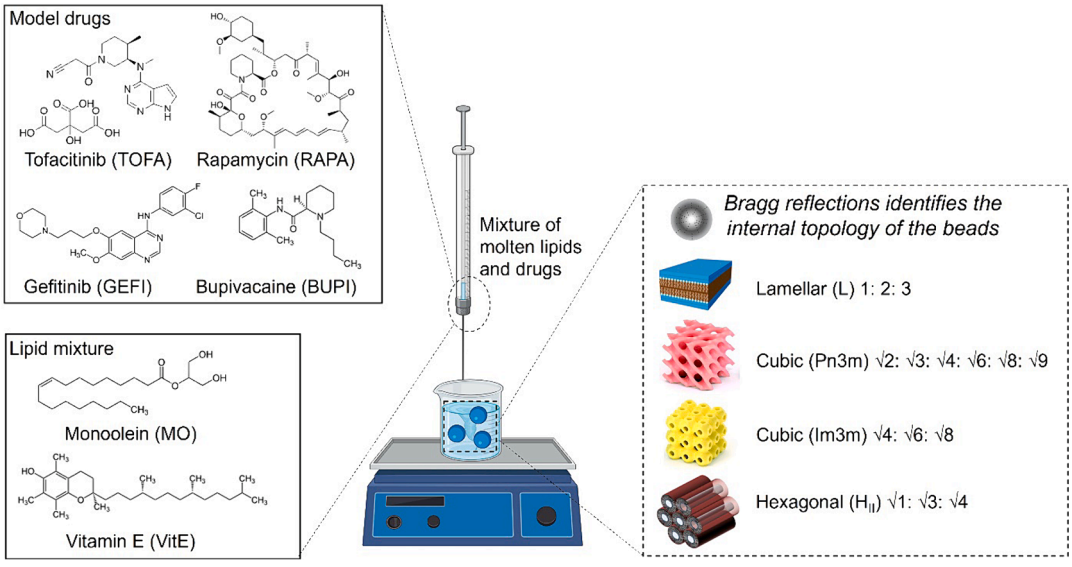


**Scheme 1.** Encapsulated drugs, monoolein (MO), and vitamin E (VitE) structures, and beads topology. Lipids in a molten state, with or without the inclusion of drugs, were introduced into a Hamilton syringe. Upon release of this mixture into a cold aqueous solution, beads were spontaneously generated. The peculiar Bragg reflections for each geometry are also reported together with a cartoon depicting the mesophase.

## 2. Experimental

Dimodan 90D (a commercial grade of lipid that contains more than 90 wt% of MO) was provided by Danisco, Denmark, as a gift and it was used as received as source of MO. TOFA and GEFI were purchased by LC laboratories (Woburn, MA), RAPA was obtained from R&S Pharmchem (Shanghai, China), BUPI hydrochloride monohydrate was obtained from Fagron (Glinde, Germany). Caffeine (Ph. Eur. Quality) and glucose monohydrate were purchased from Hänseler Swiss Pharma (Herisau, Switzerland). Trifluoroacetic acid, HEPES salt, and calcium chloride were obtained from Carl Roth (Karlsruhe, Germany). PBS tablets (140 mM NaCl, 10 mM phosphate buffer, 3 mM KCl, pH 7.4), agarose, sodium chloride, ketoconazole, lidocaine hydrochloride, vitamin E, Lipase from Candida Rugosa (4320 units/mg solid, 91,700 units/mg protein), absolute ethanol, DMSO and HPLC-grade methanol and acetonitrile were purchased by Sigma-Aldrich (USA). All the reagents were used without any further purification.

Ultrapure water of resistivity 18.2 MΩ.cm was produced by Barnstead Smart2pure (Thermo Scientific).

### 2.1. Preparation of MO-B

MO was transferred in sealed glass vials and molten at 50 °C. Subsequently, the molten lipid was loaded in a 1 mL Hamilton syringe. The lipid was then dispensed into 10 mL of cold ultrapure water at approximately 2 °C maintaining magnetic stirring at 200 rpm as described in Figure S1. For beads enriched with VitE, the molten MO was blended with either 20 % (w/w) or 45 % (w/w) of VitE, and the beads were prepared as previously described. In the case of drug-loaded beads, the molten MO was combined with TOFA, BUPI, RAPA, or GEFI at three different percentages: 0.1 % w/w (equivalent to 1 mg per 1 g), 1 % w/w (equivalent to 10 mg per 1 g), and 5 % w/w (equivalent to 50 mg per 1 g). This mixture was stirred for 30 min at 200 rpm and then sonicated (in a sonication bath; Bandelin Sonorex RK 100H) for 10 min. The resulting molten dispersion was used to create the drug-loaded beads following the previously explained procedure (Figure S1). After preparation, the beads maintain their shape, and their diameter was assessed using a Vernier caliper (1/50 mm).

### 2.2. Scanning transmission electron microscopy (STEM) analysis

Morphology and surface of the beads were examined using a Zeiss GeminiSEM 500 microscope, which was equipped with a Peltier cooling-device MK3 Cool stage from Carl Zeiss SUPRA with a working distance of about 8 mm and a high voltage of 10 kV. Analyses were conducted on hydrated systems at approximately 2 °C, employing variable pressure mode and a BSE detector (Signal A BSD4). Morphology of the de-esterified MO aggregates was analyzed using the same Zeiss GeminiSEM 500 microscope equipped with an aSTEM detector. A drop of the dispersion found in the donor compartment of the Franz cell was deposited on a copper grid (200 mesh) with an amorphous carbon film.

### 2.3. Small-Angle X-ray scattering (SAXS) and Wide-Angle X-ray scattering (WAXS)

SAXS measurements were used to evaluate the phase identity of either the empty or drug-loaded beds and to assess their swelling kinetics. To study the phase changing and its kinetics during the swelling process, beads were kept in excess of water and withdrawn at different time points (10, 20, and 30 min, 1, 2, 4, 6, 8, and 24 h) and were analyzed using SAXS, for determining the topology, the symmetry and the structural parameters (lattice and the water channel dimension) of the mesophase.[12] Moreover, since the presence of the drug may affect the phase identity, beads containing different percentages of drugs were analyzed using both SAXS and WAXS. WAXS measurements were performed to study the crystallization of the drugs once embedded in the 3D gel structure. Measurements were performed on a Bruker AXS Micro, with a microfocused X-ray source, operating at voltage and filament current of 50 kV and 1000 μA, respectively. The Cu Kα radiation (λCu Kα = 1.5418 Å) was collimated by a 2D Kratky collimator, and the data were collected by a 2D Pilatus 100 K detector (or 1D VÅNTEC-1 detector in case of WAXS). The scattering vector $Q = (4\pi/\lambda)\sin\theta$, with 2θ being the scattering angle, was calibrated using silver behenate. Data were collected and azimuthally averaged using the Saxsgui software to yield 1D intensity vs. scattering vector Q, with a Q range from 0.001 to 0.5 $Å^{-1}$ (and from 13 to 20 $nm^{-1}$ for WAXS). For all measurements, a bead was placed inside a stainless-steel cell between two thin replaceable mica sheets and sealed by an O-ring. Samples were equilibrated for 30 min before measurement, whereas scattered intensity was collected over 30 min. Measurements were performed at 25 and 37 °C. To determine the structural parameters such as the size of the water channels ($d_w$), SAXS data about the lattice (*a*) were combined with the composition of the samples. [12].

### 2.4. Rheology experiments

A stress-controlled rheometer (Modular Compact Rheometer MCR 72 from Anton Paar, Graz, Austria) was used in cone-plate geometry, 1.001° angle, and 24.967 mm diameter. The temperature control was set at 25 °C. A strain sweep was performed at 10 $s^{-1}$ between 0.001 and 100 % shear strain to determine the linear viscoelastic regime, and the yield ($\tau_y$) and flow ($\tau_f$) points. $\tau_y$ is exceeded at the point where the shear stress starts to deviate from linearity, while $\tau_f$ is represented by the shear stress value at the crossover point where G' equals G''. Both values are extrapolated from amplitude sweep graphs.

Thixotropy properties of the beads were determined by using hysterics experiments which consisted of a three-step operation: upward curve (1 % shear strain, frequency of 1 Hz), plateau curve (shear rate of 1000 $s^{-1}$) and downward curve (1 % shear strain, frequency of 1 Hz). The percentage of regeneration of MO-B and MO/VitE-B soon after their preparation was determined using the following equation:

$$\%\ of\ \ regeneration = \frac{G'\ at\ \ rest}{G'\ \ after\ \ stress}\cdot 100$$

where the values of G' at rest and G' after stress were extrapolated from the thixotropy graphs.

Experiments were conducted on beads immediately after their preparation and following 24 h of hydration. The beads were separated from water through paper filtration; for each experiment, 15 beads were placed on the rheometer plate using a spatula.

### 2.5. Differential scanning calorimetry (DSC) experiments

DSC measurements were conducted on a Mettler Toledo DSC 3 calorimeter (Mettler-Toledo International Inc., Columbus, OH, USA) to analyze the thermal behaviour and interaction of the four drugs with the MO. 40 μL aluminium pans were used. The experimental procedure designed by Efrat et al. was slightly modified:[38] samples were rapidly cooled from room temperature to −10 °C, maintaining this temperature for 10 min, and followed by gradual heating to 40 °C (rate of 2 °C/min). An empty pan was used as reference. Temperatures were determined with an accuracy of ± 0.5 °C and ΔH values with an accuracy of ±0.5 kJ/mol.

### 2.6. Quantification of the amount of drug inside each bead

Drug-loaded beads were analyzed using a Vernier caliper (1/50 mm) in order to evaluate their diameter, and, assuming they have a spherical shape, their volume. TOFA-, BUPI- and RAPA-loaded beads were dissolved in methanol (containing the proper internal standard), and centrifuged at 4 °C, 13000 rpm (18900 RCF), for 10 min. The

supernatant was analyzed using an Ultimate 3000 HPLC (Thermo Fisher Scientific, Reinach, Switzerland) and, depending on the drug, different methods were employed: TOFA,[8] BUPI,[32] and RAPA.[28]

In all cases, the concentration of the drug in the supernatant ([drug]) was evaluated using a calibration curve. Then, the amount of drug in each bead was evaluated using the following equation:

$$mg\ \ drug = [drug]\frac{Vf}{Vi}$$

where $V_f$ is the volume of MeOH we added to disrupt the beads, and $V_i$ is the volume of the spherical bead (calculated as $4\pi r^3$). GEFI-loaded beads were dissolved in DMSO, and the dispersion was analyzed using a plate reader ($\lambda$ = 333 nm). The concentration of GEFI in the mixture was evaluated using a calibration curve of GEFI in DMSO, while the amount of drug in each bead was calculated as described above.

### 2.7. Release experiments

0.1 % drug-loaded beads (3 beads) were put in an Eppendorf tube containing PBS buffer (150 mM, pH 7.4) in sink conditions (1.5 mL for the hydrophilic drugs, 2 mL for the hydrophobic drugs). Regarding RAPA, we noticed that the presence of inorganic salts in the buffer resulted in drug degradation, leading us to opt for ultrapure water instead of PBS.

Due to the solubility limit of the hydrophobic drugs, the release media was enriched with 10 % v/v of EtOH and 20 % v/v DMSO in case of RAPA- and GEFI-loaded beads, respectively. For RAPA and GEFI, we repeated some points of the experiment with 6 mL of buffer or $H_2O$ instead of 2 mL, obtaining the same results.

GEFI release was also evaluated in a simulated intraperitoneal fluid [39,40] composed of 50 mM HEPES buffer, 110 mM NaCl, 5 mM glucose and 1.68 mM $CaCl_2$ in $H_2O$/DMSO 8/2. The pH of the solution was adjusted to 7.1 units. Experiments were conducted in a shaking incubator at 100 rpm and 37 °C. At designated time points, beads were withdrawn from the solution. GEFI-loaded beads were dissolved in DMSO, and the dispersion was analyzed using a plate reader, while TOFA-, BUPI- and RAPA-loaded beads were dissolved in methanol (containing the proper internal standard), centrifuged at 4 °C, 13000 rpm (18900 RCF), for 10 min and the supernatant was analyzed using the HPLC as illustrated before, while the percentage of drug release was calculated using the following equation:

$$\%\ \ drug\ \ release = \left(1 - \frac{[drug]t}{[drug]t_0}\right) * 100$$

where $[drug]_t$ is the concentration of the drug in the beads, evaluated using a calibration curve, at desiderated time points, while $[drug]_{t0}$ is the concentration of the drug, evaluated using a calibration curve, soon after the beads preparation.

### 2.8. RAPA release experiments in simulated fluid

The release profile of RAPA was also assessed in a solution of $H_2O$/EtOH 9/1 containing 5000 units/mL of lipase from *Candida Rugosa*. For this purpose, we employed a vertical diffusion cell, with the donor compartment containing 10 beads and 7 mL of the simulated fluid, and the acceptor compartment filled with 13 mL of water enriched with 10 % of EtOH. A 500 nm filter separated the donor and acceptor compartments. At specific time points, 5 mL of the solution from the acceptor compartment were collected, replaced with fresh media, and subjected to overnight lyophilization. Subsequently, 200 μL of MeOH containing ketoconazole (200 μg/mL) were introduced, and the solution was analyzed using HPLC as previously described.

### 2.9. Free RAPA release experiments in simulated fluid

The release profile of free RAPA was assessed in a solution of $H_2O$/EtOH 9/1 containing 5000 units/mL of lipase from *Candida Rugosa*. The donor compartment of the vertical diffusion cells contained 200 μg/mL of RAPA in SF, and the acceptor compartment was filled with 13 mL of water enriched with 10 % of EtOH. A 500 nm filter separated the donor and acceptor compartments. After 24 h, the content of the acceptor compartment was analyzed using a DU 800 UV–Vis single beam spectrophotometer (Beckman Coulter). The percentage of free RAPA release after 24 h was calculated using the following equation:

$$\%drug\ \ release = \left(1 - \frac{(AbsRAPA)t}{(AbsRAPA)t_0}\right) * 100$$

where $(Abs\ RAPA)_t$ represents the absorbance of RAPA found in the acceptor compartment after 24 h, whereas $(Abs\ RAPA)_{t0}$ is the absorbance of the initial RAPA solution introduced into the donor compartment at the onset of the experiment.

### 2.10. Particle tracking analysis

Particle size measurements were conducted utilizing a Nanosight NS300 instrument with a blue laser ($\lambda$ = 488 nm). Samples, collected from the donor compartment of the vertical diffusion cells and diluted 10 times with ultrapure water, were introduced into the instrument cell using a syringe pump with a flow rate of 50 μL/s. Five acquisitions, each lasting 60 s and capturing 25 frames/s, were performed.

### 2.11. RAPA stability over time

A solution of RAPA in $H_2O$/EtOH 9/1 containing or not 5000 units/mL of lipase from *Candida Rugosa* was analyzed during time using a DU 800 UV–Vis single beam spectrophotometer (Beckman Coulter), both at room temperature and 37 °C.

### 2.12. Erosion test

The evaluation of the bead erosion in buffers containing 10% EtOH or 20% DMSO was conducted using a precision analytical balance. The beads were left in ultrapure water for a day, reaching a Pn3m phase that could not swell anymore. Subsequently, they were filtered and individually placed in Eppendorf tubes for weighing. To evaluate the erosion, 2 mL of a buffer enriched with the respective organic solvent was added to each bead. After a predetermined set time, the solvent was removed, and each bead was filtered and weighed once again. The percentage of erosion was evaluated using the following equation:

$$\%erosion = \left(1 - \frac{(mg)t}{(mg)t_0}\right) * 100$$

where $(mg)_t$ is the weight of the bead after a set time of contact with the enriched buffer, while $(mg)_{t0}$ is the initial weight of the bead.

### 2.13. Release experiments in agarose gel

Agarose gel was used to mimic living tissues;[41] it was produced by dissolving 0.5 % w/v agarose in water (100 mg/20 mL), the mixture was then subjected to a microwave (700 W) for 20 s. Once the agarose solution reached approximately 55 °C, 0.5 mL of it was transferred into a 5 mL Eppendorf tube, which was kept at 4 °C for 5 min to allow gel formation. 9 BUPI-loaded beads were introduced into the agarose gel and subsequently covered with an additional 0.5 mL of agarose solution. After 5 min at 4 °C, the added agarose solution solidified into a gel and 1.5 mL of PBS buffer were added on the top of the gel. Experiments were conducted in a shaking incubator at 100 rpm and 37 °C.

At designated time points, the release medium was completely

replaced with fresh PBS buffer and aliquots were taken for lyophilization. Each sample was resuspended with internal standard solution (lidocaine) in methanol, and drug content was analyzed by HPLC as explained before. The percentage of cumulative drug release was evaluated using the following equation:

$$\%\ drug\ \ release = \left(\frac{mgBUPIt}{mgBUPIt_0}\right) * 100$$

where mg $_{BUPI\ t}$ represents the mg of the drug found in the release medium after the lyophilization, while mg $_{BUPI\ t0}$ represents the mg of BUPI loaded in the beads soon after their preparation.

### 2.14. Injectability of the beads

Injectability of the beads was tested using an 18G needle. In our case, a 1 mL disposable syringe was loaded with 15 beads, and they were injected into cold ultrapure water (2 °C) in a beaker (Figure S2a) and in agarose gel (Fig. S2b). As shown, beads were extruded and did not maintain their shape.

**Statistical Analysis**: Quantification of the amount of drug in each bead was carried out with n > 20 in all cases, while other experiments were carried out in triplicates. Data in all cases are expressed as means ± SD. All calibration curves showed a $R^2 > 0.998$. Microsoft Excel was used for general calculations, while GraphPad Prism 9.5 and SigmaPlot 12 were used for plotting.

## 3. Results and discussion

### 3.1. Morphology of the beads

Among the various bio-inspired materials available to form depot injectables, we selected LMPs, a class of materials belonging to the lyotropic-liquid–crystal family, possessing a tunable three-dimensional nanostructure along with peculiar mechanical and rheological properties. By altering the water content and temperature or incorporating additives, we tailored the LMPs to exhibit lamellar, cubic, inverse hexagonal, or micellar geometries. Although already extensively investigated - either as bulk gel or as colloidal dispersion - to achieve controlled drug release, LMP-based formulations have not been reported so far as starting material to manufacture beads. Here, MO was chosen as main lipid and it was blended with different percentages of the antioxidant VitE [10–15] which, acting as a stiffener of lipid chains, can promote the formation of highly viscous inverted micellar and hexagonal phases.[16] Adding 20 % (w/w) or 45 % (w/w) of VitE to the formulation allowed us to achieve $H_{II}$ and inverse micelle-based beads, structures that MO alone could not form. However, while the $H_{II}$-based beads (MO/VitE-B) are stable and maintain their shape over time, the others exhibited instability and a tendency to aggregate within a brief time, limiting their application as drug delivery systems.

The spherical nature of the beads and their mean diameter (≈ 3 mm) is evident in the optical microscope pictures (Fig. 1b and 1e), while scanning transmission electron microscope (STEM) put in evidence that the surface roughness is more pronounced in pure MO based-beads (MO-B; Fig. 1c and d) compared to the smoother and gel-like texture of MO/VitE-B (Fig. 1d and g). In both cases, the production process allowed us to obtain batches with low variability in terms of size and weight (Fig. 1h and 1i).

### 3.2. Topology and properties of the beads

Since the beads were formed by dropping molten lipids in water, to deepen our knowledge of the internal structure and symmetry of the beads at different hydration times, and thus gain information about the kinetics of swelling, we investigated changes in mesophase structure and transitions between different LMPs by SAXS measurements. The X-ray beam directed at the gel results in a scattering pattern with a set of maxima that correspond to sharp Bragg reflections characteristic of the long-range positional order. Each Bragg reflection is reported above each peck, and a list of Bragg reflections identifying the symmetry of the mesophase are reported in figure captions, too. Moreover, to determine structural parameters such as the size of the water channels ($d_w$), SAXS data about the lattice (*a*) were combined with the composition of the samples as described.[12] According to Fig. 2a, MO-B exhibited a lamellar phase between 10 and 20 min of hydration. Subsequently, a transition to an Ia3d phase occurred and it is completed in 10 min, while after 2 h the gel reached a fully hydrated Pn3m phase, in agreement with the phase diagram of MO.[19,42] The swelling process of MO-B during time could be noticed by naked eye, as shown in Figure S3: L beads are milky-white, Ia3d beads show transparent sides, while Pn3m beads are entirely transparent. The lattice parameters (*a*; which refers to the

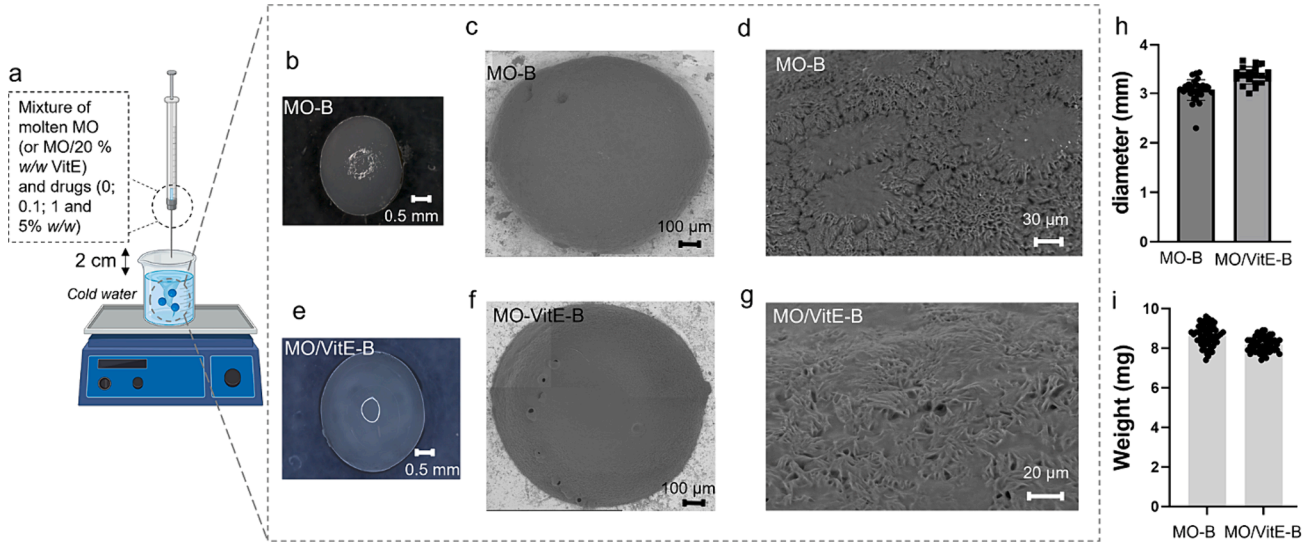


**Fig. 1.** A) Schematic representation of the beads preparation, (b) representative optical microscopy image of monoolein based-beads (MO-B), c) and d) STEM image of MO-B at 15x magnification and 300x magnification, respectively, e) optical microscope image of MO/VitE-B, f) and g) scanning transmission electron microscope (STEM) image of MO/VitE-B at 15x magnification and 433x magnification, respectively, h) MO-B and MO/VitE-B diameter (n = 30) and i) MO-B and MO/VitE-B weight (n = 55). The beads' diameter was evaluated using a Vernier caliper (1/50 mm), while the beads' weight was evaluated using an analytical balance.

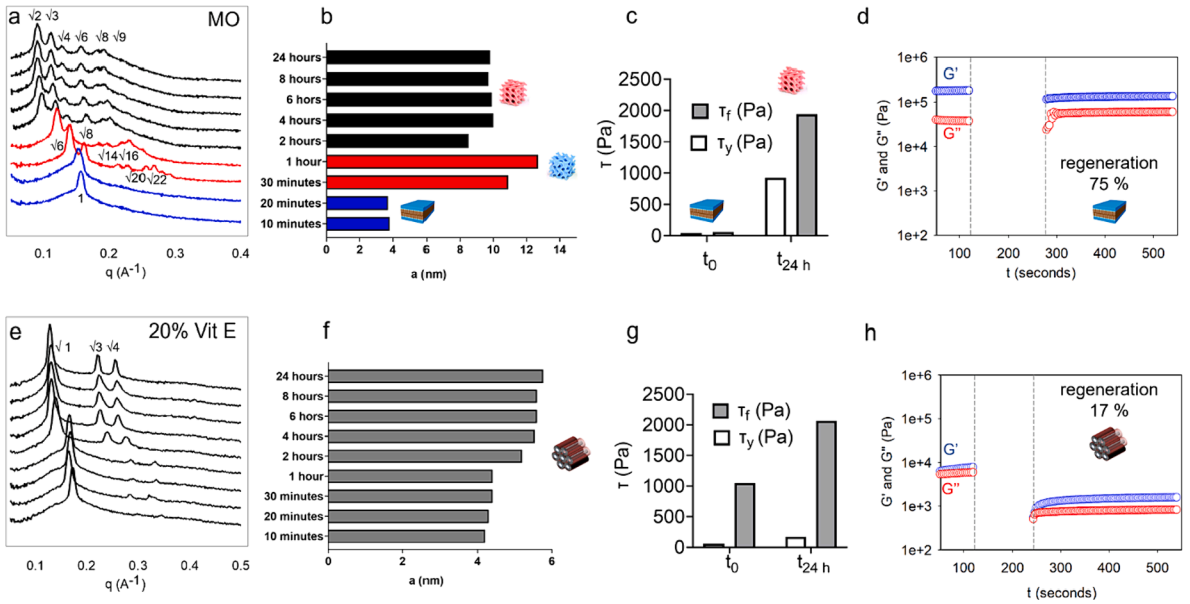


**Fig. 2.** A) Change of the internal geometry of MO-B evaluated by SAXS experiments among 24 h of equilibration in excess of water and b) the lattice parameters derived from SAXS spectra, c) flow point ($\tau_f$) and yield point ($\tau_y$) values of MO-B soon after the preparation and after 24 h of equilibration in excess of water, d) thixotropy experiments of MO-B soon after their preparation, e) change of the internal geometry of MO/VitE-B evaluated by SAXS experiments among 24 h of equilibration in excess of water and f) the lattice parameters derived from SAXS spectra. The Bragg reflections for the $H_{II}$ ($\sqrt{1}$: $\sqrt{3}$: $\sqrt{4}$), L (1: 2: 3: 4), Ia3d (($\sqrt{6}$: $\sqrt{8}$: $\sqrt{14}$: $\sqrt{16}$: $\sqrt{20}$: $\sqrt{22}$) and Pn3m ($\sqrt{2}$: $\sqrt{3}$: $\sqrt{4}$: $\sqrt{6}$: $\sqrt{8}$: $\sqrt{9}$) phases are reported above each peak. g) flow ($\tau_f$) and yield point ($\tau_y$) values of MO/VitE-B soon after the preparation and after 24 h of equilibration in excess of water, h) thixotropy experiments of MO/VitE-B soon after their preparation.

spacing between repeating structural units) are *ca.* of 3 nm for the L phase, 11 nm for the Ia3d phase and roughly 9 nm for the Pn3m phase (Fig. 2b), while the water channel diameter ($d_w$) is approximately 2.5 nm and 4 nm for the Ia3d phase and the Pn3m phase, respectively (Figure S4), in good agreement with the bulk gel parameters reported in the literature.[19] Upon the addition of 20 % (w/w) of VitE to MO, the beads promptly exhibit a stable $H_{II}$ phase yet after 10 min, with a lattice of approximately 5 nm (Fig. 2e and 2f) as expected from literature reports.[15] Despite the instability observed in beads composed of MO/VitE 55/45, we successfully identified an inverse micellar phase after 2 h (Figure S5), in analogy with what observed in the bulk gel.[43].

While SAXS gave information about a short-range order, rheology measurements enabled us to predict the relation among stress, strain, and the rate of deformation of materials to characterize the mechanical properties of the beads. All the beads (independently from their hydration) show a shear thinning behaviour (Figure S6) and the shape of G′ and G″ (the storage and loss of moduli, respectively) exhibit a sharp downturn at the limit of the linear viscoelastic region (LVR). Above that, a strain increase causes the disruption of the network, resulting in a decrease of both G′ and G″ as evident in the representative amplitude sweep experiments (Figure S6). Flow ($\tau_f$) and yield point ($\tau_y$) values, both related to the required force to be applied on the sample to induce flow, put in evidence that less hydrated beads (*i.e.* soon after their preparation) exhibit lower elasticity than the more hydrated ones, indicating that the beads are more easily injectable soon after their preparation (Fig. 2c and 2 g, respectively). More interestingly, considering that the shear during this process can affect the strength and the viscosity of the beads, thixotropy experiments (which refers to the time-dependent changes in viscosity or flow behaviour of a material when subjected to repeated cycles of shear stress or deformation) were also conducted. The results demonstrate that soon after preparation MO-B exhibited a regeneration rate of 75 %, whereas MO/VitE-B a regeneration rate of 17 % (Fig. 2d and 2 h, respectively). The underlying mechanism involves the reversible breakdown and reformation of structural elements within the material in the case of MO-B, while an important loss in regeneration was observed in the case of $H_{II}$ beads. This information is critical for designing effective drug delivery systems that maintain their structural integrity, ensuring consistent and predictable drug release profiles: the injection of $H_{II}$ beads could potentially result in the loss of their 3D structure, leading to a concurrent alteration in drug release dynamics.

### 3.3. Topology and properties of drugs-loaded beads

To assess the suitability of the beads as a drug delivery platform, we loaded four model drugs with different polarity, physicochemical properties, mechanisms of action, and routes of administration at three distinct initial ratios (0.1 %, 1 %, and 5 % w/w with respect to MO): the hydrophilic TOFA and BUPI, as well as the hydrophobic GEFI and RAPA. As expected, loaded beads maintained the same diameter as the unloaded ones (≈ 3 mm, Figure S7) and SAXS analysis (carried out after 24 h of hydration) demonstrated that the inclusion of TOFA, GEFI, and RAPA did not influence either the phase identity of the formulations (that remained all in Pn3m phase, as shown in Fig. 3a, 3c, and 3d, respectively) or their structural parameters (Fig. 3e, g and h).

As TOFA is a hydrophilic molecule and we anticipated a significant release rate from cubic based-beads, we decided to load the drug into $H_{II}$ beads (MO/VitE-B) as well; also in this case, TOFA did not induce any changes in the structure of the beads, as demonstrated with the SAXS experiments reported in Fig. 3i.

Interestingly, when 5 % (w/w) of drugs was loaded into the beads (Pn3m or $H_{II}$), SAXS patterns also showed a reflection at high q (circles in Fig. 3) that cannot be attributed to a Bragg's reflection. Moreover, the presence of reflections in the WAXS spectra suggested indeed that this was due to the drug crystals (Figure S8). Differently, in the case of BUPI-loaded beads, an Im3m phase was obtained after 24 h of hydration for all three ratios (Fig. 3b). We hypothesize that the amphiphilic nature and/or its highest polarity/water solubility caused its redistribution between the polar interface and the hydrophobic domains during hydration, with the consequent formation of a primitive symmetry. Similarly, the loading of BUPI in glycerol monooleate systems caused a phase transition from Pn3m to $H_{II}$ structures, as literature reports.[44] Structural parameters also varied: lattice reached 18 nm while $d_w$ increased up to 8 nm (Fig. 3f) exceeding the value commonly observed in Im3m

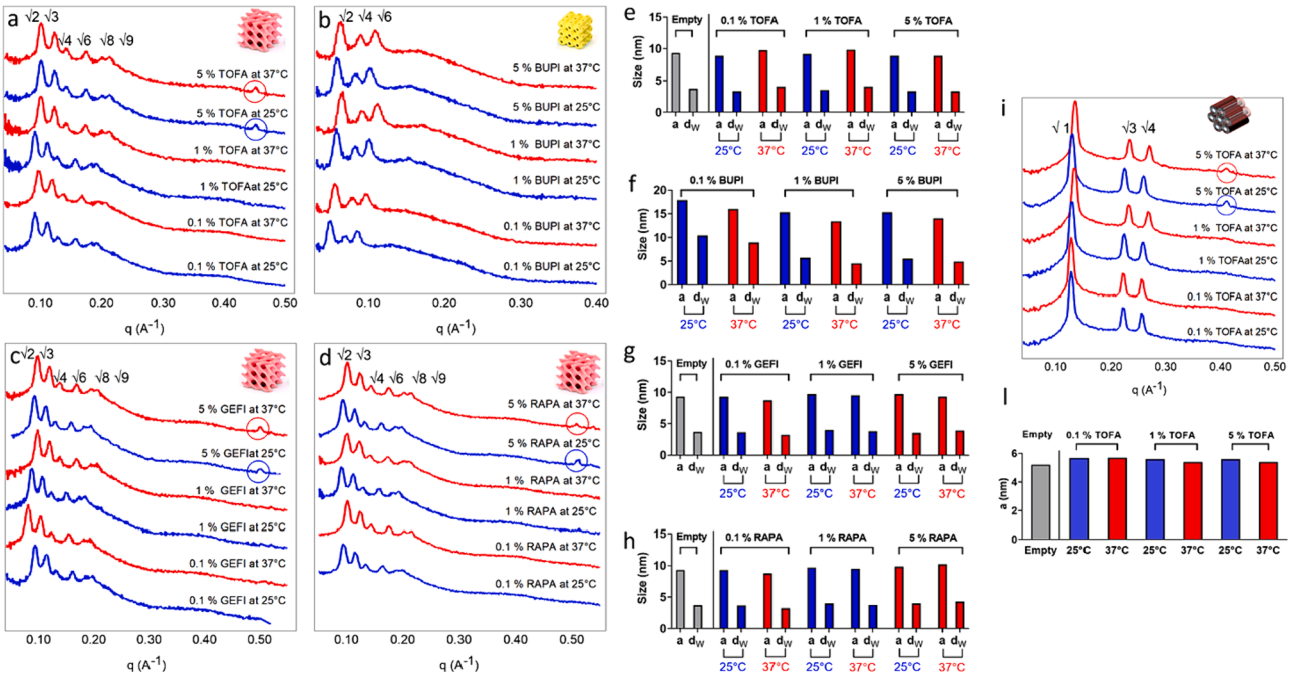


**Fig. 3.** A) SAXS spectra of (a) TOFA-, (b) BUPI-, (c) GEFI- and (d) RAPA-loaded beads at different ratios (0.1 %, 1 % and 5 % w/w); e) Lattice parameter (a) and water channel dimension ($d_w$) values of TOFA-, f) BUPI-, g) GEFI- and h) RAPA-loaded beads at different ratios (0.1 %, 1 % and 5 % w/w), i) SAXS spectra of MO/VitE-B loaded with TOFA at different ratios (0.1 %, 1 % and 5 % w/w), l) a and $d_w$ values of MO/VitE-B loaded with TOFA at different ratios (0.1 %, 1 % and 5 % w/w). The Bragg reflections for the $H_{II}$ ($\sqrt{1}$: $\sqrt{3}$: $\sqrt{4}$), Pn3m ($\sqrt{2}$: $\sqrt{3}$: $\sqrt{4}$: $\sqrt{6}$: $\sqrt{8}$: $\sqrt{9}$) and Im3m ($\sqrt{4}$: $\sqrt{6}$: $\sqrt{8}$) phases are reported above each peak.

symmetry.[19] The absence of a reflection peak in the SAXS spectra at high q (Fig. 3b) and in the WAXS spectra (Figure S8) indicates that, differently from the other drugs, BUPI was in its amorphous state even when present at the highest ratio (5 % w/w). Moreover, the topology of the mesophases (and their structural parameters) remains unaffected by temperature variations as evident from SAXS and WAXS analyses conducted at both 25 °C and 37 °C.

Our platform demonstrated the capacity to effectively vehiculate substantial quantities of drugs, achieving a remarkable entrapment efficiency exceeding 80 % for both hydrophilic and hydrophobic drugs (Figure S9): starting from 0.1 %, 1 % or 5 % formulations (1 mg, 10 mg, or 50 mg drug/1g of MO), each bead entrapped approximately 8 μg, 80 μg or 380 μg of the drug, respectively (Figure S9). Such high entrapment efficiency translates to a reduced requirement of formulation during administration and may result in a decrease in the frequency of administration, enhancing patient compliance.

**Table 1**
DSC parameters of MO-B and MO/VitE-B, loaded or not. ΔH values are expressed in J/g, while $T_m$ values are expressed in °C. Error in the case of the obtained temperatures and ΔH are within 0.5 °C and 1.5 J/g, respectively (averaged over three measurements). * Averaged Tm value.

| | | L | | Ia3d | | Pn3m | | Im3m | | $H_{II}$ | |
|---|---|---|---|---|---|---|---|---|---|---|---|
| | | ΔH | $T_m$ | ΔH | $T_m$ | ΔH | $T_m$ | ΔH | $T_m$ | ΔH | $T_m$ |
| **MO-B** | | 58.8 | 12.8* | 45.9 | 12.3 | 23.0 | 11.8 | | | | |
| **TOFA** | **0.1 %** | 23.9 | 12.5 | | | 38.9 | 12.4 | | | | |
| | **1 %** | 49.7 | 12.9 | | | 39.5 | 11.6 | | | | |
| | **5 %** | 20.7 | 12.5 | | | 36.7 | 11.4 | | | | |
| **BUPI** | **0.1 %** | 50.6 | 12.7 | | | | | 37.6 | 12.6 | | |
| | **1 %** | 28.8 | 12.1 | | | | | 38.9 | 11.1 | | |
| | **5 %** | 40.8 | 10.5 | | | | | 36.8 | 11.0 | | |
| **GEFI** | **0.1 %** | 40.6 | 12.2 | | | 36.5 | 11.5 | | | | |
| | **1 %** | 44.3 | 12.6 | | | 24.9 | 11.0 | | | | |
| | **5 %** | 19.3 | 11.2 | | | 27.5 | 10.8 | | | | |
| **RAPA** | **0.1 %** | 46.9 | 11.6 | | | 39.4 | 12.7 | | | | |
| | **1 %** | 41.6 | 12.3 | | | 40.1 | 11.2 | | | | |
| | **5 %** | 18.2 | 11.7 | | | 33.7 | 11.6 | | | | |
| **MO/VitE-B** | | | | | | | | | | 38.8 | 15.5 |
| **TOFA** | **0.1 %** | | | | | | | | | 5.3 | 14.3 |
| | **1 %** | | | | | | | | | 7.0 | 12.8 |
| | **5 %** | | | | | | | | | / | / |

Differential scanning calorimetry (DSC) allows to determine the enthalpy changes associated with the phase transition and the temperatures at which it occurs. Before recording the heating thermograms, we incubated each sample below zero degrees to reduce the risk of undercooling of water in hydrated MO and to stabilize the L phase (when present).[45] Thermograms of MO-B (Figure S10a) for each topology showed endothermic transitions between 10 and 15 °C.[45] In the case of the L phase, it is evident that the main peak is broad and split into two peaks of similar magnitude, with Tm values of 11 and 14 °C. The ΔH values associated with the observed peaks, reported in Table 1, are relatively small, as typically observed for these systems.[45,46] In case of Pn3m phase (23 J/g), ΔH values were sensibly lower than the L (58 J/g) or Ia3d (46 J/g) phases. It is reasonable to hypothesize that the higher the curvature radius and the tortuosity of the aqueous channel network, the lower the strength of the interaction among lipids in the bilayer. As a consequence, even though the Pn3m phase is distinguished by high lipid packing, it exhibits the lowest ΔH value, while the Ia3d phase demonstrates an intermediate value. Upon adding 20 % of VitE to the formulation ($H_{II}$ phase), the peak broadens and the ΔH value becomes similar to that of the Pn3m phase (Table 1).

When the percentage of VitE is further increased to 45 %, the transition is completely abolished. This is not surprising, given that lipid organization is different in the corresponding micellar phase, leading to very weak interactions among lipid chains due to their low compaction. DSC measurements on loaded beads were conducted to investigate the effect of the four drugs on lipid bilayer structure and its dependence on their percentage (Figure S10b – S10l). In the presence of drugs, the shape of the peak in the DSC thermogram remains mostly unchanged, but variations in ΔH values (reported in Table 1) occur.

Specifically, when MO-B is in Pn3m phase (the most hydrated one), the ΔH value increases by at least 10 J/g (doubling with 0.1 % and 1 % of RAPA). The Im3m phase obtained in the presence of BUPI shows comparable results. These findings suggest that the presence of a drug in the most hydrated MO-B structure leads to lipid compaction regardless of their structure and polarity. However, when MO-B is in the L phase, the presence of drugs causes a reduction in ΔH values, which varies depending on their nature and amount. For instance, the presence of 5 % of hydrophobic molecules such as RAPA and GEFI results in a three-fold decrease in ΔH values, indicating that these drugs, by penetrating the hydrophobic region of the mesophase in its L geometry, perturbed lipid packing and reduced their compaction. The hydrophilic drug TOFA, when present at 0.1 % and 5 %, caused a 50 % decrease in ΔH values compared to the corresponding MO-B without drugs, whereas at 1 % of TOFA the reduction was only 15 %. The shape of the thermograms (Figure S10b) for 0.1 % and 5 % of the drug is remarkably similar to the split thermogram of empty MO-B. On the other hand, at 1 %, the main peak of TOFA is centred at about 13 °C with a shoulder at lower temperatures (≈ 8 °C), indicating that this specific ratio induces a change in bilayer organization leading to a noticeable increase in lipid compaction (reflected in higher ΔH and Tm values). In the case of $H_{II}$ beads, TOFA abolished the phase transition even at low ratio, likely because the drug further hindered the weak interactions between lipid chains (Figure S10, panel l).

The presence of 0.1 % of the other hydrophilic drug BUPI in L phase leads to the same reduction obtained in the presence of TOFA but, in this case, the lowest ΔH value was observed in the beads containing 1 % of the drug (Figure S10, panel c).

The effect of BUPI on bilayer organization is contingent on its concentration in the beads: at 0.1 %, it induces the least significant variations, evidenced by the smallest reduction in ΔH values compared to empty MO-B and beads loaded with the same amount of other drugs. When BUPI concentration reaches 1 %, the ΔH value is halved compared to MO-B and is significantly lower than beads containing 1 % of other drugs. At 5 %, BUPI induces a unique bilayer organization (similar to TOFA): evident phase separation appears in the thermogram, a new main peak emerges at a lower temperature (≈ 10.5 °C) and the ΔH value is the highest compared to beads containing 5 % of other molecules. It is possible that BUPI's non-crystalline behaviour in the beads, unlike the other drugs, contributes to this anomalous behaviour.

Overall, these results indicate that hydrophilic drugs interact differently with MO when it is in the L phase, likely because TOFA and BUPI, featuring distinct moieties and polarity, are localized in different portions of the lipid bilayer due to specific interactions between the functional groups of the drugs and the polar head of MO.

### 3.4. Release profile of drugs and injectability of the beads

Evaluating the release profiles of drugs is crucial to assess the efficacy of any drug delivery platform and different mechanisms (such as diffusion, erosion or swelling) may drive the drug release.

Although we employed different experimental conditions to overcome drugs' solubility (and instability) issues and to mimic the physiological conditions, all the dissolution media does not affect the internal structure of the mesophases (see SI; Figure S11), while, as reported below, either the swelling process or the erosion of the beads have an impact on the drug release. Primarily, the release mechanisms of actives are influenced by the mesophase's structure (topology and aqueous channels diameter) and drug size and polarity. In general, their diffusion coefficient ($d$) decreases with the dimensionality of the topology [19], with the cubic phases displaying the highest diffusion coefficients ($d = 3$), the L and $H_{II}$ phases showing an intermediate one ($d = 2$ and $d = 1$, respectively) [16]. However, in our setup, immediately after the preparation of the beads, they were submerged in an excess of media and the release profiles of the four drugs were determined starting from the less hydrated beads (since they could be easily injected) which intake water leading to a dynamic phase changing during the experiment. Thus, we cannot use the above-mentioned paradigm to describe the release profile. Indeed, our drugs do not follow a Fickian diffusion profile and, consequently, the release profile cannot be modelled using the Higuchi equation. Moreover, we also observed gel erosion and therefore, we do not reject the hypothesis that the release process can be driven by a combination of diffusion, swelling and gel dissolution process.

TOFA was quickly released (more than 85 % after 7 h) in physiological conditions (PBS buffer, 150 mM, pH 7.4, Fig. 4a). Therefore, to decrease the drug release rate, thus achieving a sustained release, we loaded TOFA in $H_{II}$ beads, since this mesophase is characterized by a lower $d$ with respect to Pn3m phase. In this case, as assumed, the percentage of drug release decreased: after an initial burst, 85 % of release was achieved after six days instead of a few hours (Fig. 4a) despite a loss in regeneration was observed (see Fig. 2h). Thus, although these beads do not maintain their structural integrity, they ensure a consistent and predictable drug release profile.

The injectability of the proposed MO-B was tested using a syringe and an 18G needle, both in aqueous solution and in an agarose gel system that mimicked a subcutaneous injection:[41] in both cases, they were extruded (Figure S2, S14). In particular, we analysed MO-B soon after their injection in aqueous solution with SAXS, and it revealed that L phase changed to an Ia3d one (Figure S11). In order to study if this phase change could cause any variations in the release profile of a molecule, we tested it using TOFA as model drug.

The release profile of TOFA from extruded beads (Ia3d phase, light grey bars in Fig. 4b) after one h is quite different from the one obtained with beads soon after their preparation (L phase, black bars in Fig. 4b). After one day, instead, the release profiles were similar. This result is not surprising since L phase displays a lower $d$ than cubic phases. To prove this hypothesis, we investigated the release of TOFA from beads that remained 24 h in an aqueous solution saturated with the drug, which has a Pn3m symmetry (dark grey bars in Fig. 4b). TOFA release from Pn3m beads after 1 h and 1 day is quite similar to the release from Ia3d beads, meaning that the extrusion process could have influenced the release profile of TOFA in the first hours.

The release profile of GEFI was also assessed, both in physiological

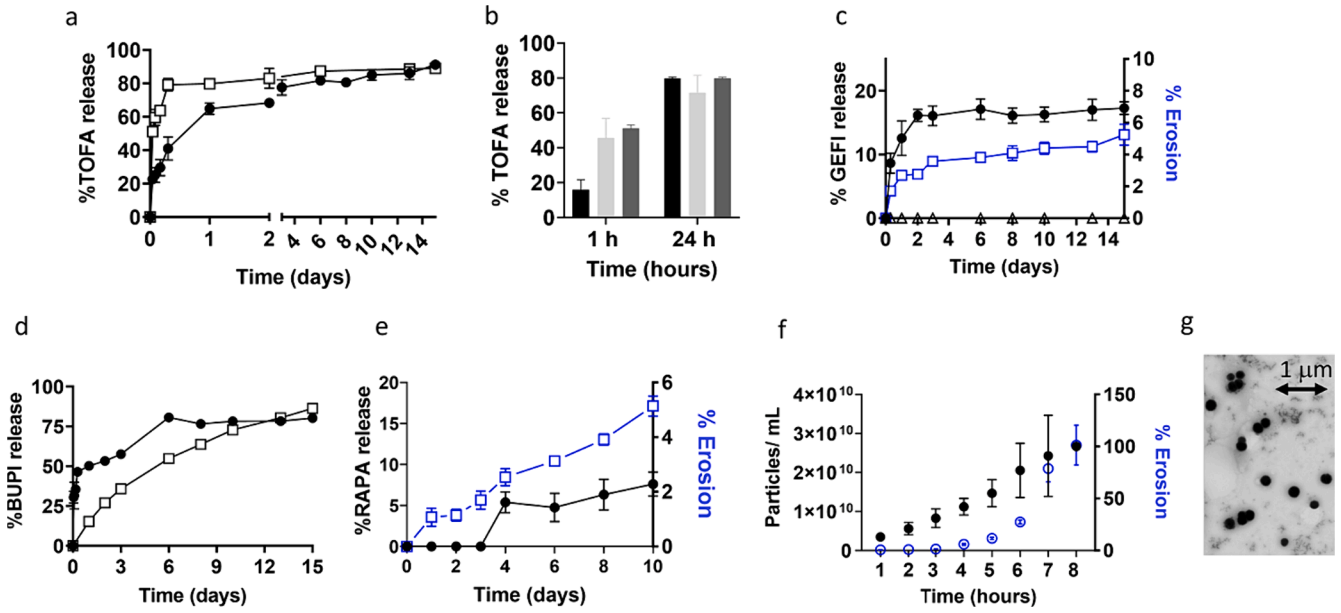


**Fig. 4.** A) Release profile of TOFA in physiological conditions from MO-B (white squares) and MO/VitE-B (black dots), b) comparison of release profile of TOFA from beads after preparation (black bars), after injection (light grey bars) and in their Pn3m phase (dark grey bars), c) release profile of GEFI in physiological conditions (white triangles), in SF (black dots) together with the erosion of the beads in the SF (squares; right axis), d) release profile of BUPI in physiological conditions (black dots) and from agarose gel (white squares), e) release profile of RAPA in $H_2O$/EtOH 9/1 (black dots) together with the erosion of the beads in the same media (squares; right axis), f) erosion of RAPA-loaded beads in SF (blue frame circles; left axis) and formation of de-esterified MO aggregates (black circles; right axis) during time and g) STEM images of aggregates composed of de-esterified MO. Each measurement is expressed as mean ± STDV. (n = 3). (For interpretation of the references to colour in this figure legend, the reader is referred to the web version of this article.)

conditions and in a simulated intraperitoneal fluid (20 % of DMSO was added to bypass drug solubility limit). In the first case, GEFI was not released from the beads, even after 15 days, while in simulated intraperitoneal environment the percentage of drug released reached the 20 % (Fig. 4c). Both buffers enriched with DMSO did not affect the mesophase of the beads (Pn3m), as pointed out by SAXS experiments (Figure S11), but the presence of glucose in simulated fluid (SF) leads to 5 nm water channel. Sugar esters are usually added to lipids to enlarge water channels;[47] probably glucose was incorporated into the beads during the swelling process and interacted with the polar heads of MO with consequent formation of expanded water channels. GEFI is a small molecule so it should pass through channels of 3 nm and should not need extended ones, but it is reasonable to think that their enlargement encourages its release because of the highest amount of water in the channels.

MO exhibits partial solubility in DMSO, so the drug release can be influenced by both diffusion and erosion mechanisms. Hence, we assessed the percentage of erosion of the beads in the buffer enriched with the organic solvent during time and it's lower than 5 %: that means that GEFI release is mostly driven by diffusion processes and not by the erosion of the system (Fig. 4c).

Despite the Im3m phase had a $d = 3$ and BUPI is well soluble in water, its release profile in physiological conditions was sensitively slower than those obtained with TOFA's Pn3m beads (Fig. 4d). Likely, non-covalent interactions between the drug and MO were established, as supported by the formation of an Im3m phase instead of a Pn3m one, reducing its ability to leave the aqueous channels. The release profile of BUPI was also assessed an agarose gel-based system, that mimics the subcutaneous environment[41] (where BUPI-loaded beads should be administered) limiting unnecessary animal experimentation in the first stages of a study. Fig. 4d points out the sustained and controlled release of BUPI over time in subcutaneous environment, indicating the good potentiality of the proposed delivery system.

On the other hand, RAPA release in physiological conditions (enriched with 10 % of EtOH for solubility reasons) was mostly driven by erosion (Fig. 4e): in this case release and erosion profiles were very similar and they reached about 15 % release in 15 days. The presence of EtOH had no impact on the topology of the beads and they continued to maintain their Pn3m phase, while the presence of lipase (that mimic inflammation) in SF led to a $H_{II}$ topology, as revealed by SAXS experiments (Figure S11). Moreover, macroscopically, RAPA-loaded beads had completely eroded after 8 h in SF, reasonably because lipases hydrolysed the ester bond of MO. Lipase, in fact, is an enzyme that catalyses the hydrolysis of triacylglycerols by breaking the ester bonds between the glycerol and the fatty acid molecules.[48] The degradation of glyceryl monooleate, a LMPs precursor with a structural resemblance to MO, induced by lipase has previously been reported.[49]

The release profile of RAPA in SF was evaluated using a vertical diffusion cell. We expected to achieve a complete release of the drug after 8 h since we observed the disruption of the beads, but no RAPA was detected in the acceptor compartment of the diffusion cells. To ensure that lipases did not degrade RAPA, obstructing its visibility in the HPLC chromatograms, we checked the stability of the drug in the presence of the enzyme over time. The UV–Vis spectra revealed a 5 nm redshift within one day, observed at both room temperature and 37 °C. Notably, this redshift persisted even in the absence of lipases, ruling out the enzyme as the cause (Figure S12). It is likely that the hydrophobic RAPA experienced aggregation or formed complexes with other molecules in a such polar environment ($H_2O$/EtOH 9/1), inducing alterations in the electronic structure and consequential spectral shifts. Over the course of two weeks, no changes were discerned, indicating that RAPA retained stability in the solution in the presence of the enzyme (see Figure S12). We also examined the ability of free RAPA to cross the membrane from the donor compartment to the acceptor compartment: after 24 h, nearly all the drug (≈ 78 %) was found in the acceptor compartment, meaning that no interactions with the membrane or the diffusion cell hindered the drug from being detected in the acceptor compartment. To further investigate, we analysed the content of the donor compartment tracking the species dissolved into the SF and, surprisingly, we discovered a predominant population of aggregates of 150 nm in diameter

(Figure S13, panel a) after one hour. Within one day, this population became heterogeneous, ranging from 150 to 400 nm in diameter (Figure S13b - S13d). As shown in Fig. 4f, the higher the erosion of the beads during time, the greater the number of aggregates they formed. These vesicles were probably composed of de-esterified MO that rearranged itself into spherical vesicles, encapsulating the hydrophobic RAPA. STEM images of the aggregates found in the donor compartment after 8 h are reported in Fig. 4g. Despite the complete erosion of the beads, the aggregates they form act as a sustained drug delivery system. We monitored the vesicle size in SF for two weeks, observing gradual aggregation that led to the formation of different populations with sizes ranging from 150 to 900 nm. Some representative distribution images are reported in Figure S13e – S13i. The aggregation was also confirmed by assessing the vesicle concentration in the dispersion, revealing a gradual decrease in the number of particles per millilitres over time within 10 days (Figure S13, panels f and g). After this time, the concentration remained stable, as the distribution of the vesicles (Figure S13, panels h and i).

## 4. Conclusions

We reported, for the first time, the preparation of LMPs-based beads as a platform for the local and sustained release of drugs. Ranging from hydrophilic to hydrophobic compounds, we demonstrated that excellent loading efficiency can be obtained and that a sustained release profile for the four distinct drugs we tested could be achieved. Following comprehensive physicochemical characterization, we showed that, despite the complete erosion of the beads in the presence of lipase - typically present in cells and tissues of patients with inflammatory diseases - the degradation product of MO can reorganize and create spherical aggregates that continue to function as drug delivery systems.

Our LMP-based beads hold great promises as an injectable drug delivery system and, by means of future *in vivo* studies, we plan to fully harness their therapeutic potential.

## CRediT authorship contribution statement

**Elena Allegritti:** Writing – original draft, Visualization, Validation, Investigation, Formal analysis, Data curation. **Luisa Giansanti:** Writing – review & editing, Supervision, Methodology, Formal analysis. **Gregor Bordon:** Methodology. **Maria Anna Maggi:** Resources, Methodology. **Paola Luciani:** Writing – review & editing, Supervision, Project administration, Funding acquisition, Conceptualization. **Simone Aleandri:** Writing – original draft, Visualization, Validation, Methodology, Investigation, Formal analysis, Data curation, Conceptualization.

## Declaration of competing interest

The authors declare that they have no known competing financial interests or personal relationships that could have appeared to influence the work reported in this paper.

## Data availability

Data will be made available on request.

## Acknowledgements

We kindly thank Dr. Lorenzo Arrizza (Center of Microscopy of the University of L'Aquila, Italy) for his support with STEM image acquisition. Remo Eugster (Department of Chemistry, Biochemistry and Pharmaceutical Sciences, University of Bern) is acknowledged for his support during the setup of the agarose system. Professor Raffaele Mezzenga and Dr. Serena Rosa Alfarano (Laboratory of Food & Soft Materials, Institute of Food, Nutrition and Health, IFNH; Department for Health Sciences and Technology, D-HEST, ETH Zurich Switzerland) are kindly acknowledged for the precious support during the SAXS experiments.

## Appendix A. Supplementary material

Supplementary data to this article can be found online at https://doi.org/10.1016/j.jcis.2024.03.067.

## References

[1] H.M.G. Barriga, M.N. Holme, M.M. Stevens, Cubosomes: the next generation of smart lipid nanoparticles? Angew. Chemie - Int. Ed. 58 (2019) 2958–2978, https://doi.org/10.1002/anie.201804067.
[2] J. Zhai, C. Fong, N. Tran, C.J. Drummond, Non-lamellar lyotropic liquid crystalline lipid nanoparticles for the next generation of nanomedicine, ACS Nano. 13 (2019) 6178–6206, https://doi.org/10.1021/acsnano.8b07961.
[3] D.P. Chang, J. Barauskas, A.P. Dabkowska, M. Wadsäter, F. Tiberg, T. Nylander, Non-lamellar lipid liquid crystalline structures at interfaces, Adv. Colloid Interface Sci. 222 (2015) 135–147, https://doi.org/10.1016/j.cis.2014.11.003.
[4] R. Mezzenga, J.M. Seddon, C.J. Drummond, B.J. Boyd, G.E. Schröder-Turk, L. Sagalowicz, Nature-inspired design and application of lipidic lyotropic liquid crystals, Adv. Mater. 31 (2019) 1900818, https://doi.org/10.1002/adma.201900818.
[5] S. Phan, W.K. Fong, N. Kirby, T. Hanley, B.J. Boyd, Evaluating the link between self-assembled mesophase structure and drug release, Int. J. Pharm. 421 (2011) 176–182, https://doi.org/10.1016/j.ijpharm.2011.09.022.
[6] O. Elzenaty, P. Luciani, S. Aleandri, A lipidic mesophase with tunable release properties for the local delivery of macromolecules: the apoferritin nanocage, a case study, J. Mater. Chem. b. (2022) 3876–3885, https://doi.org/10.1039/d2tb00403h.
[7] C.M. Chang, R. Bodmeier, Effect of dissolution media and additives on the drug release from cubic phase delivery systems, J. Control. Release. 46 (1997) 215–222, https://doi.org/10.1016/S0168-3659(96)01596-9.
[8] M. Carone, M.R. Spalinger, R.A. Gaultney, R. Mezzenga, K. Hlavačková, A. Mookhoek, P. Krebs, G. Rogler, P. Luciani, S. Aleandri, Temperature-triggered in situ forming lipid mesophase gel for local treatment of ulcerative colitis, Nat. Commun. 14 (2023) 3489, https://doi.org/10.1038/s41467-023-39013-3.
[9] J. Clogston, M. Caffrey, Controlling release from the lipidic cubic phase. amino acids, peptides, proteins and nucleic acids, J. Control. Release. 107 (2005) 97–111, https://doi.org/10.1016/j.jconrel.2005.05.015.
[10] Y.-D. Dong, I. Larson, T. Hanley, B.J. Boyd, Bulk and dispersed aqueous phase behavior of phytantriol: effect of vitamin E acetate and F127 polymer on liquid crystal nanostructure, Langmuir. 22 (2006) 9512–9518, https://doi.org/10.1021/la061706v.
[11] L. Bitan-Cherbakovsky, I. Yuli-Amar, A. Aserin, N. Garti, Structural rearrangements and interaction within H(II) mesophase induced by cosolubilization of vitamin E and ascorbic acid, Langmuir. 25 (2009) 13106–13113, https://doi.org/10.1021/la901195t.
[12] R. Mezzenga, C. Meyer, C. Servais, A.I. Romoscanu, L. Sagalowicz, R.C. Hayward, Shear rheology of lyotropic liquid crystals: a case study, Langmuir. 21 (2005) 3322–3333, https://doi.org/10.1021/la046964b.
[13] G. Montalvo, M. Valiente, E. Rodenas, Rheological properties of the L phase and the hexagonal, lamellar, and cubic liquid crystals of the CTAB/BENZYL alcohol/water system, Langmuir. 12 (1996) 5202–5208, https://doi.org/10.1021/la9515682.
[14] N.M. Bandarra, R.M. Campos, I. Batista, M.L. Nunes, J.M. Empis, Antioxidant synergy of α-tocopherol and phospholipids, J. Am. Oil Chem. Soc. 76 (1999) 905–913, https://doi.org/10.1007/s11746-999-0105-4.
[15] L. Sagalowicz, S. Guillot, S. Acquistapace, B. Schmitt, M. Maurer, A. Yaghmur, L. De Campo, M. Rouvet, M. Leser, O. Glatter, Influence of vitamin e acetate and other lipids on the phase behavior of mesophases based on unsaturated monoglycerides, Langmuir. 29 (2013) 8222–8232, https://doi.org/10.1021/la305052q.
[16] I. Martiel, N. Baumann, J.J. Vallooran, J. Bergfreund, L. Sagalowicz, R. Mezzenga, Oil and drug control the release rate from lyotropic liquid crystals, J. Control. Release. 204 (2015) 78–84, https://doi.org/10.1016/j.jconrel.2015.02.034.
[17] M. Ramezanpour, M.L. Schmidt, B.Y.M. Bashe, J.R. Pruim, M.L. Link, P.R. Cullis, P. E. Harper, J.L. Thewalt, D.P. Tieleman, Structural properties of inverted hexagonal phase: a hybrid computational and experimental approach, Langmuir. 36 (2020) 6668–6680, https://doi.org/10.1021/acs.langmuir.0c00600.
[18] J.M. Seddon, J. Robins, T. Gulik-Krzywicki, H. Delacroix, Inverse micellar phases of phospholipids and glycolipids, Phys. Chem. Chem. Phys. 2 (2000) 4485–4493, https://doi.org/10.1039/b004916f.
[19] S. Aleandri, R. Mezzenga, The physics of lipidic mesophase delivery systems, Phys. Today. 73 (2020) 38–44, https://doi.org/10.1063/PT.3.4522.
[20] J. Zhao, B. Guo, P.X. Ma, Injectable alginate microsphere/PLGA-PEG-PLGA composite hydrogels for sustained drug release, RSC Adv. 4 (2014) 17736–17742, https://doi.org/10.1039/c4ra00788c.
[21] Y. Huang, S. Gui, Factors affecting the structure of lyotropic liquid crystals and the correlation between structure and drug diffusion, RSC Adv. 8 (2018) 6978–6987, https://doi.org/10.1039/c7ra12008g.
[22] Y. Almoshari, Development, therapeutic evaluation and theranostic applications of cubosomes on cancers: an updated review, Pharmaceutics 14 (2022) 600, https://doi.org/10.3390/pharmaceutics14030600.

[23] S. Aleandri, D. Bandera, R. Mezzenga, E.M. Landau, Biotinylated cubosomes: a versatile tool for active targeting and codelivery of paclitaxel and a fluorescein-based lipid dye, Langmuir. 31 (2015) 12770–12776, https://doi.org/10.1021/acs.langmuir.5b03469.
[24] B. Feagon, Update on Tofacitinib for Inflammatory Bowel Disease, Gastroenterol. Hepatol. 12 (2016) 572–574.
[25] V. Molander, H. Bower, T. Frisell, B. Delcoigne, D. Di Giuseppe, J. Askling, Venous thromboembolism with JAK inhibitors and other immune-modulatory drugs: a Swedish comparative safety study among patients with rheumatoid arthritis, Ann. Rheum. Dis. 82 (2022) 189–197, https://doi.org/10.1136/ard-2022-223050.
[26] K. Migita, K. Eguchi, T. Aoyagi, T. Tsukada, M. Tsuboi, Y. Kawabe, S. Nagataki, The effects of the immunosuppressant rapamycin on the growth of rheumatoid arthritis (RA) synovial fibroblast, Clin. Exp. Immunol. 104 (1996) 86–91, https://doi.org/10.1046/j.1365-2249.1996.d01-651.x.
[27] A. Perl, Activation of mTOR (mechanistic target of rapamycin) in rheumatic diseases, Nat. Rev. Rheumatol. 12 (2016) 169–182, https://doi.org/10.1038/nrrheum.2015.172.
[28] G. Bordon, S.N. Ramakrishna, S.G. Edalat, R. Eugster, A. Arcifa, M. Vermathen, S. Aleandri, M.F. Bertoncelj, J. Furrer, P. Vermathen, L. Isa, R. Crockett, O. Distler, P. Luciani, Liposomal aggregates sustain the release of rapamycin and protect cartilage from friction, J. Colloid Interface Sci. 650 (2023) 1659–1670, https://doi.org/10.1016/J.JCIS.2023.07.087.
[29] G. Bordon, F. Berenbaum, O. Distler, P. Luciani, Harnessing the multifunctionality of lipid-based drug delivery systems for the local treatment of osteoarthritis, Biomed. Pharmacother. 168 (2023) 115819, https://doi.org/10.1016/j.biopha.2023.115819.
[30] C.D. Cho, G.A. Fisher, J. Halsey, B.I. Sikic, Phase I study of gefitinib, oxaliplatin, 5-fluorouracil, and leucovorin (IFOX) in patients with advanced solid malignancies, Invest. New Drugs. 24 (2006) 117–123, https://doi.org/10.1007/s10637-006-2032-7.
[31] R.J. Cersosimo, Gefitinib: an adverse effects profile, Expert Opin. Drug Saf. 5 (2006) 469–479, https://doi.org/10.1517/14740338.5.3.469.
[32] S. Aleandri, L. Rahnfeld, D. Chatzikleanthous, A. Bergadano, C. Bühr, C. Detotto, S. Fuochi, K. Weber-Wilk, S. Schürch, P. van Hoogevest, P. Luciani, Development and in vivo validation of phospholipid-based depots for the sustained release of bupivacaine, Eur. J. Pharm. Biopharm. 181 (2022) 300–309, https://doi.org/10.1016/j.ejpb.2022.11.019.
[33] R. Eugster, A.A. Ganguin, A. Seidi, S. Aleandri, P. Luciani, 3D printing injectable microbeads using a composite liposomal ink for local treatment of peritoneal diseases, Drug Deliv. Transl. Res. (2023), https://doi.org/10.1007/s13346-023-01472-y.
[34] P.A. Moore, Bupivacaine: a long-lasting local anesthetic for dentistry, Oral surgery, Oral Med. Oral Pathol. 58 (1984) 369–374, https://doi.org/10.1016/0030-4220(84)90325-6.
[35] M.A. Paganelli, G.K. Popescu, Actions of bupivacaine, a widely used local anesthetic, on NMDA receptor responses, J. Neurosci. 35 (2015) 831–842, https://doi.org/10.1523/JNEUROSCI.3578-14.2015.
[36] T. Halaszynski, Bupivacaine, Essence Analg. Analg. (2010) 274–276. https://doi.org/10.1017/CBO9780511841378.065.
[37] L. Bitan-Cherbakovsky, I. Yuli-Amar, A. Aserin, N. Garti, Solubilization of vitamin e into HII LLC mesophase in the presence and in the absence of vitamin C, Langmuir. 26 (2010) 3648–3653, https://doi.org/10.1021/la903100m.
[38] R. Efrat, E. Kesselman, A. Aserin, N. Garti, D. Danino, Solubilization of hydrophobic guest molecules in the monoolein discontinuous QL cubic mesophase and its soft nanoparticles, Langmuir. 25 (2009) 1316–1326, https://doi.org/10.1021/la8016084.
[39] N. Gitlin, J.L. Stauffer, R.C. Silvestri, The pH of ascitic fluid in the diagnosis of spontaneous bacterial peritonitis in alcoholic cirrhosis, Hepatology. 2 (1982) 408S–411S, https://doi.org/10.1002/hep.1840020403.
[40] P. Bhusal, J.L. Rahiri, B. Sua, J.E. McDonald, M. Bansal, S. Hanning, M. Sharma, K. Chandramouli, J. Harrison, G. Procter, G. Andrews, D.S. Jones, A.G. Hill, D. Svirskis, Comparing human peritoneal fluid and phosphate-buffered saline for drug delivery: do we need bio-relevant media? Drug Deliv. Transl. Res. 8 (2018) 708–718, https://doi.org/10.1007/s13346-018-0513-9.
[41] C. Bassand, J. Verin, M. Lamatsch, F. Siepmann, J. Siepmann, How agarose gels surrounding PLGA implants limit swelling and slow down drug release, J. Control. Release. 343 (2022) 255–266, https://doi.org/10.1016/j.jconrel.2022.01.028.
[42] C.V. Kulkarni, W. Wachter, G. Iglesias-Salto, S. Engelskirchen, S. Ahualli, Monoolein: a magic lipid? Phys. Chem. Chem. Phys. 13 (2011) 3004–3021, https://doi.org/10.1039/c0cp01539c.
[43] M. Kumar, G. Kumaraswamy, Phase behaviour of the ternary system: monoolein-water-branched polyethylenimine, Soft Matter. 11 (2015) 5705–5711, https://doi.org/10.1039/c5sm01082a.
[44] A. Angelova, V.M. Garamus, B. Angelov, Z. Tian, Y. Li, A. Zou, Advances in structural design of lipid-based nanoparticle carriers for delivery of macromolecular drugs, phytochemicals and anti-tumor agents, Adv. Colloid Interface Sci. 249 (2017) 331–345, https://doi.org/10.1016/j.cis.2017.04.006.
[45] H. Qiu, M. Caffrey, The phase diagram of the monoolein/water system: metastability and equilibrium aspects, Biomaterials. 21 (2000) 223–234, https://doi.org/10.1016/S0142-9612(99)00126-X.
[46] C.W. Reese, Z.I. Strango, Z.R. Dell, S. Tristram-Nagle, P.E. Harper, Structural insights into the cubic-hexagonal phase transition kinetics of monoolein modulated by sucrose solutions, Phys. Chem. Chem. Phys. 17 (2015) 9194–9204, https://doi.org/10.1039/c5cp00175g.
[47] R. Negrini, R. Mezzenga, Diffusion, molecular separation, and drug delivery from lipid mesophases with tunable water channels, Langmuir. 28 (2012) 16455–16462, https://doi.org/10.1021/la303833s.
[48] C.T. Hou, Y. Shimada, Lipases, Encycl. Microbiol. Third Ed. (2009) 385–392. https://doi.org/10.1016/B978-012373944-5.00153-X.
[49] L. Mei, H. Wang, J. Chen, Z. Zhang, F. Li, Y. Xie, Y. Huang, T. Peng, G. Cheng, X. Pan, C. Wu, Self-assembled lyotropic liquid crystal gel for osteoarthritis treatment: via anti-inflammation and cartilage protection, Biomater. Sci. 9 (2021) 7205–7218, https://doi.org/10.1039/d1bm00727k.